

# Status of the ATLAS Detector and results from commissioning with cosmic rays and single beams<sup>†</sup>

*Luis Hervas, on behalf of the ATLAS collaboration  
CERN, PH Dept.  
1211 Geneva 23, Switzerland*

## Abstract

*We report on operation and performance studies of the ATLAS detector with large samples of cosmic-ray events collected during 2008 and first single LHC beam data in September 2008. Emphasis will be placed on the performance of the calorimeter system, relevant for measurements in many physics processes.*

## 1 Introduction

The ATLAS collaboration has built a general purpose detector to be operated at the LHC proton-proton collider at CERN. Section 2 of this paper briefly covers the construction and installation of the different sub-detectors and other components of ATLAS. For several years, an important commissioning effort has been on-going. Data-taking with cosmic muons has been pursued since 2005 when the first sub-detectors were partially installed in the ATLAS pit. In September 2008, first events produced by single proton beams circulating in the LHC and colliding on collimators, were recorded with the detector. These data have been used to commission the detector for operation before collisions and to perform important tasks such as detector alignment, channel mapping, verification of operational stability and noise studies. Selected examples of this work will be briefly described in Section 3.

## 2 Detector Description

The ATLAS detector is a general purpose instrument designed to study proton-proton collisions at the LHC collider. It is composed of a tracking system to detect and measure the momentum of charged particles, a calorimeter system to measure the energy of electromagnetic and hadronic particles and a large-volume magnetic tracking system to detect and measure high energy muons escaping the calorimeters. All systems cover as much as possible the full solid angle around the interaction point. A full description of the ATLAS detector is collected in Ref.[1] and many references therein.

The requirements, initial specifications and conceptual design of the sub-detectors were laid out in the early 1990's, followed by beam tests and a long period of research, development and prototyping. The series production of the different parts and sub-detectors extended from the late 1990's to early 2000's, overlapping with the detector

---

<sup>†</sup>Presentation at HEP-MAD09, 21-28th August 2009, Antananarivo, Madagascar

installation in the ATLAS cavern at the LHC point 1 which began in 2003 and continued until the first closure for beam in summer 2008. In total, this corresponds to an almost 20 year-long effort

A cut-away view of the detector is shown in Figure 1. The detector occupies the whole ATLAS cavern and is approximately 44 m long and 25 m high and weighs 7000 tonnes. It has been installed piece by piece directly underground.

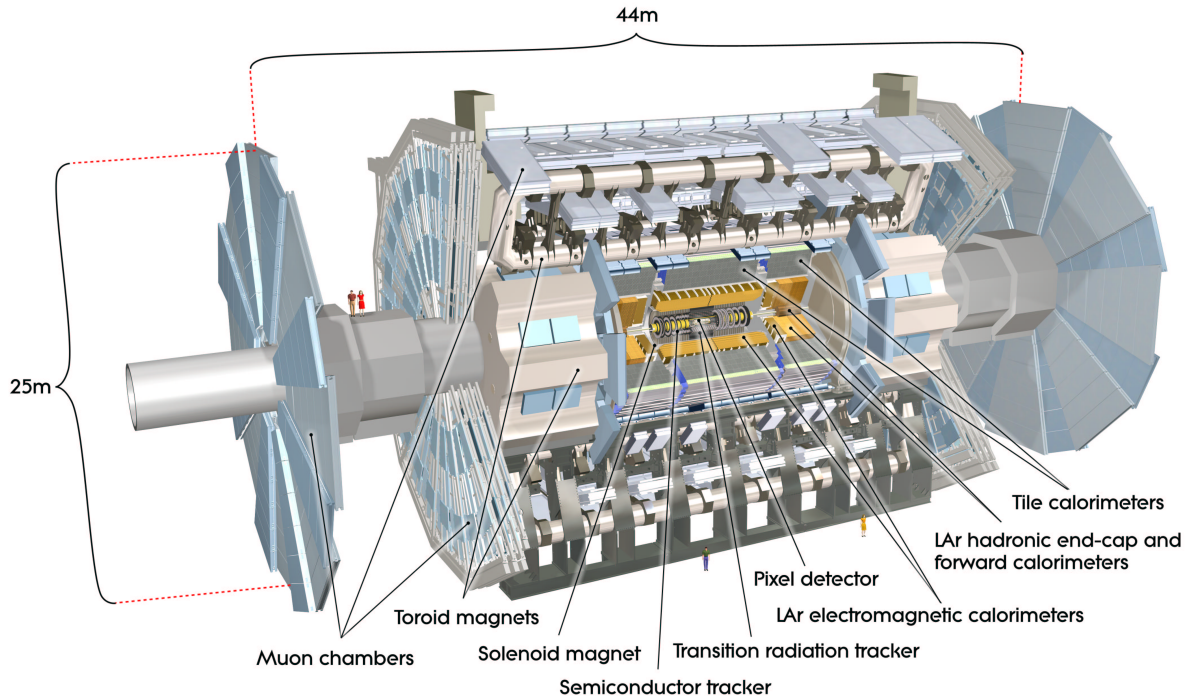


Figure 1: *Cut-away view of the ATLAS detector. The detector is approximately 44 m long, 25 m high and weighs 7000 tonnes.*

Table 1 summarises the main design parameters and performance goals for each detector component. Each major component is described in the following sections.

Detector component	Required resolution	$\eta$ coverage	
		Measurement	Trigger
Tracking	$\sigma_{p_T}/p_T = 0.05\% p_T \oplus 1\%$	$\pm 2.5$	
Electromagnetic calorimetry	$\sigma_E/E = 10\%/\sqrt{E} \oplus 0.7\%$	$\pm 3.2$	$\pm 2.5$
Hadronic calorimetry (jets)			
Barrel and end-cap	$\sigma_E/E = 50\%/\sqrt{E} \oplus 3\%$	$\pm 3.2$	$\pm 3.2$
Forward	$\sigma_E/E = 100\%/\sqrt{E} \oplus 10\%$	$3.1 <  \eta  < 4.9$	$3.1 <  \eta  < 4.9$
Muon spectrometer	$\sigma_{p_T}/p_T = 10\%$ at $p_T = 1$ TeV	$\pm 2.7$	$\pm 2.4$

Table 1: *Main design parameters and performance goals for each ATLAS detector component. The units for  $E$  and  $p_T$  are in GeV.*

## 2.1 Inner Detector

The inner detector (ID) of ATLAS is composed of three sub-detectors to cope with the large number of particles emerging from the interaction point (IP). The whole system (a cylinder of 6 m length and 2 m diameter) is housed and supported in the bore of the

barrel calorimeter cryostat, in a volume with a 2T magnetic field parallel to the beam axis. A cut-away view of the ID is shown in Figure 2.

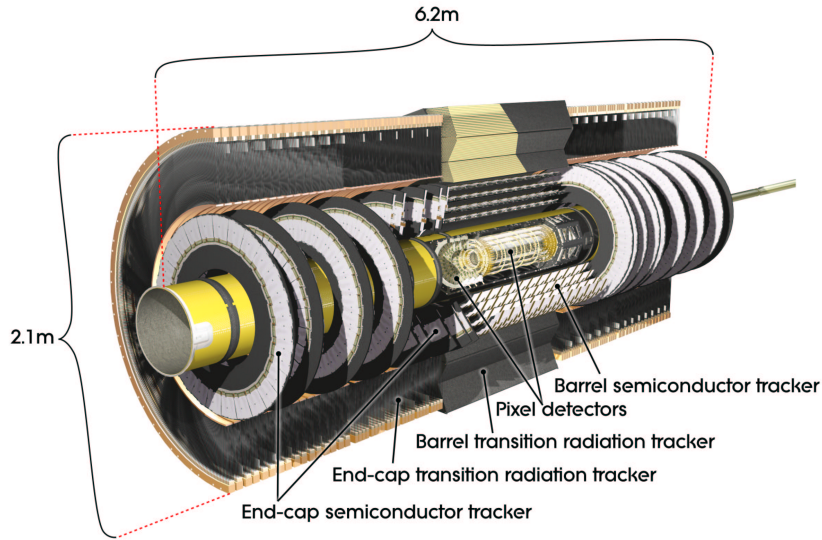


Figure 2: *Cut-away view of the ATLAS inner detector. One can see the cylindrical structures (barrel) and the disks (end-caps) for each of the three different sub-detectors.*

The innermost detector, at radii between 5 and 12 cm from the IP, the so-called pixel detector consists of three layers of silicon modules (assembled as cylinders in the barrel and as disks on each end-cap side), segmented in  $R - \phi$  and  $z$  with a minimum pixel size of  $50 \times 400 \mu\text{m}^2$ . A track typically crosses three layers. The pixel detector has approximately 80.4 million readout channels.

At radii between 30 and 50 cm, charged particles are measured in the Semiconductor Tracker (SCT), where normally four space-points are measured on each track using four double (at small stereo angle) layers of microstrip silicon detectors. The strips are typically 12.8 cm long (two 6.4 cm modules bonded together) with a pitch of  $80 \mu\text{m}$ . The detector modules are also assembled as cylinders in the barrel and as disks in each end-cap. The SCT has approximately 6.3 million readout channels.

Further away from the IP, the Transition Radiation Tracker (TRT) made of 4.4 mm diameter straws interleaved with transition-radiation radiator material provides typically 36 points per track and particle identification between electrons and pions in the range between 0.5 and 150 GeV. The straw modules (barrel) and wheels (end-caps) are located at radii between 55 and 107 cm. The TRT has approximately 351.000 readout channels.

The ID has a coverage in pseudo rapidity over  $|\eta| < 2.5$  (the TRT covers only over  $|\eta| < 2.0$ ) and a momentum resolution  $\sigma_{p_T}/p_T = 0.05\% p_T \oplus 1\%$ . With the combination of highly granular measurements at small radii and many coarser measurements at larger radii, the ID provides high precision measurements in both the  $R - \phi$  and  $z$  coordinates, robust pattern recognition to measure tracks, as well as excellent secondary vertexing and particle identification performance.

## 2.2 Calorimeters

The calorimeter system of ATLAS surrounds the ID volume over  $|\eta| < 4.9$ . Different technologies and granularities are used to match the wide variety of physics requirements. The total containment ( $11 \lambda$ ) is sufficient to measure high-energy jets and to operate the outer muon spectrometer with minimal punch-through.

A cut-away view of the calorimeter system is shown in Figure 3 depicting the different barrel and end-cap regions, as well as the different detector technologies.

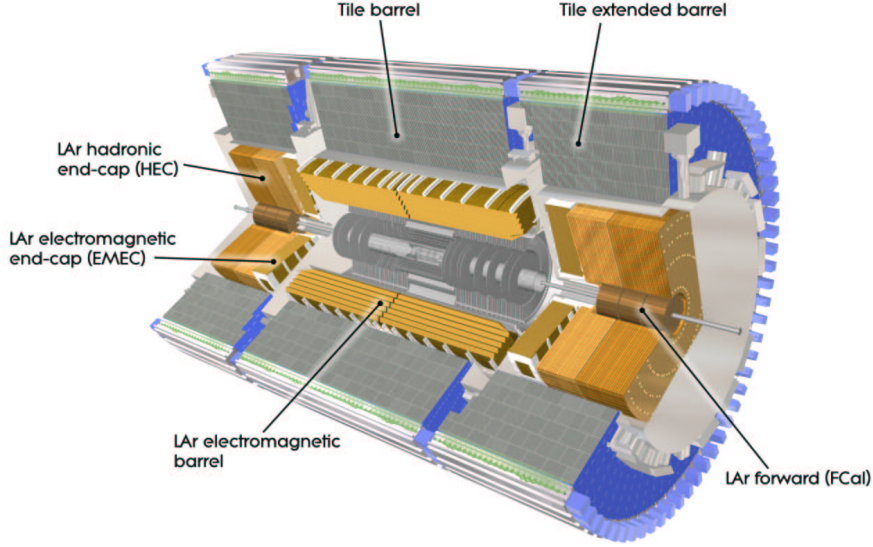


Figure 3: *Cut-away view of the ATLAS calorimeter system with its various electromagnetic and hadronic components.*

The electromagnetic (EM) calorimeter, consists of a barrel ( $|\eta| < 1.475$ ) and two end-cap parts ( $1.375 < |\eta| < 3.2$ ), in three separate cryostats. The central solenoid is integrated into the barrel cryostat to minimize the material in front of the EM calorimeter. The EM calorimeter is built as layers of liquid argon (LAr) for the active material and lead for the absorbers shaped following an accordion-like geometry. The granularity of the detector is achieved by etching charge collection pads of different sizes on the electrodes in the LAr and ganging together different layers, thus forming readout cells. These electrodes have three layers in depth. The first layer has a very fine granularity in the  $\eta$ -direction to determine the  $\eta$ -direction of photons and optimize the  $\gamma/\pi^0$  separation. The middle layer collects most of the energy deposited by EM showers and has a granularity of  $0.025 \times 0.025$  in  $\eta - \phi$  space. A presampler detector located in the LAr in front of the calorimeter provides an additional handle to measure the energy lost in the material in front of the EM calorimeter. The detailed (and complex) granularities of the different layers as a function of  $\eta$  can be found in Refs. [1] and [2].

The hadronic calorimeter has a central part (up to  $|\eta| < 1.7$ ) consisting of steel as the absorber and of scintillating tiles as the active material, called the Tile calorimeter, and two end-caps consisting of the Hadronic End Caps, (HEC) covering  $1.5 < |\eta| < 3.2$  with LAr as active medium and copper absorbers and of the Forward Calorimeters (FCal) covering  $3.1 < |\eta| < 4.9$  with tungsten absorbers. The Tile calorimeter is organized into a barrel section and two extended barrels, each one made of 64 wedge shaped modules. Each HEC calorimeter is made of two wheels, each wheel composed of 32 wedge shaped modules, and is located in the same cryostat as the EM end-cap counterpart. The FCal calorimeters are also integrated into the end-cap cryostats to minimize dead areas, but are recessed by more than one meter from the front of the EM end-cap to reduce the neutron albedo in the ID volume. To cope with the high particle fluxes expected at high  $\eta$  the FCal has very thin (0.2-0.5 mm) LAr gaps instead of the typical gap sizes of 2 mm in the EM and of 1.8 mm in the HEC.

The number of calorimeter readout channels is approximately 180 thousand in the LAr part (with about 170 thousand for the EM presampler and calorimeters and ten thousand for the HEC and FCal) and ten thousand for the Tile part.

In addition to the measurements expected for the different objects, as shown in Table 1, the calorimeter plays a major role at all levels of the trigger of the experiment and in particle identification (electrons, photons, hadronic decays of  $\tau$ -leptons, muons), jets and missing transverse energy.

## 2.3 Magnet System

The magnet system of ATLAS is a superconducting system operating at liquid Helium temperature. It is composed of several distinct parts. The central solenoid is located in the bore of the LAr barrel cryostat and generates a 2 T field parallel to the beam axis which returns via the iron structure of the Tile calorimeter. The outer muon system is arranged inside a magnetic field produced by three toroidal magnet systems. The barrel toroid (BT) consists of eight 25 m long race-track shaped coils, each one in its own cryostat. The two end-cap toroids (ECT) also consist of eight coils each, located however in a single cryostat and rotated by  $22.5^\circ$  in  $\phi$  with respect to the BT coils. The BT system provides the mechanical structure to support the large muon chambers and all services in that region. The ECT systems are the heaviest (240 tonnes) single objects lowered into the cavern. The bending power generated by the toroid magnets is between 1 and 7 Tm depending on the  $\eta$  position.

## 2.4 Muon Spectrometer

The muon spectrometer includes two full systems, fast chambers for triggering at the Level-1 in the ATLAS data acquisition and precision tracking chambers. The fast chambers are resistive-plate chambers (RPC) in the barrel region ( $|\eta| < 1.05$ ) and thin gap chambers (TGC) in the end-caps ( $1.05 < |\eta| < 1.7$ ). Their time resolution is less than 10 ns and have 2 dimensional readout with spatial resolution in the 5-10 mm range. For precision readout, monitored drift tubes (MDT) chambers are used in the barrel area ( $|\eta| < 2.7$ ) and cathode strip chambers (CSC) in the end-cap part ( $2.0 < |\eta| < 2.7$ ). As an example, for the MDT chambers, the spatial resolution is in the range  $35 - 40\mu\text{m}$ , using several (3-8) layers of tubes per chamber. Typically three layers of chambers are crossed by the muons. A cross-section of the barrel and end-cap chambers can be seen in Figure 4.

The design value for the momentum resolution for high energy muons is  $\sigma_{p_T}/p_T=10\%$  at  $p_T = 1$  TeV, equivalent to a sagitta of about  $500\mu\text{m}$  to be measured with a resolution  $\leq 50\mu\text{m}$ . To keep this resolution over the whole volume in absolute and relative positioning of the layers, precise mechanical assembly and a sophisticated optical alignment system are needed. Additionally a continuously monitoring system with 1800 Hall probes measures the magnetic field in the spectrometer volume. These values are compared to magnetic-field simulations which allow to correct for the exact position of the coils and the perturbations of the iron induced by the iron in Tile calorimeter and other metallic structures.



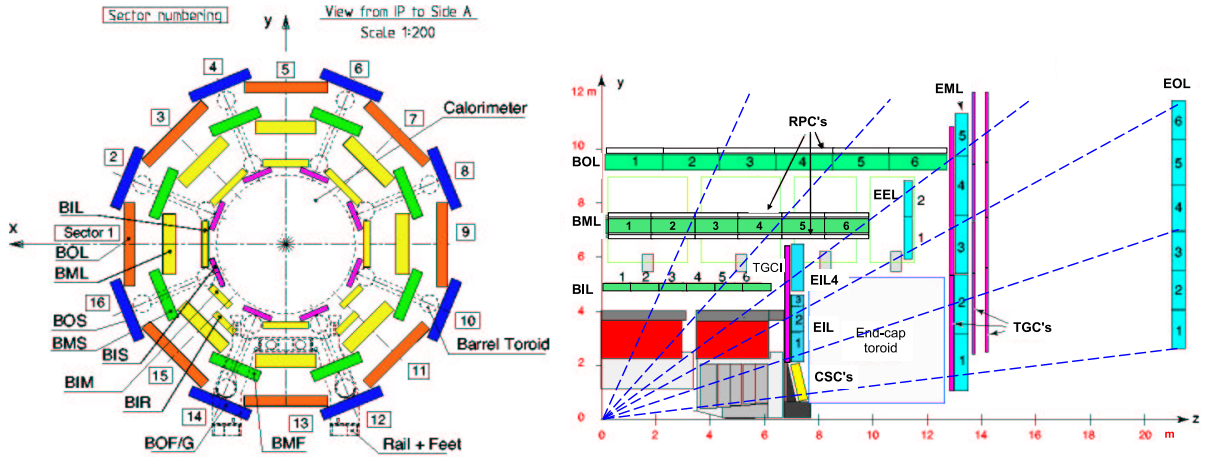


Figure 4: *Cross-sections of the ATLAS muon spectrometer layout, shown perpendicular to the beam axis (left) and in the bending plane along the beam axis (right). The different acronyms indicate the chamber technologies (see text) and layer locations.*

## 2.5 Forward Detectors

In the very forward regions, are located several small detectors which play an important role in ATLAS. The LUCID detectors (LUminosity measurement using Cerenkov Integrating Detector) at  $\pm 17$  m from the IP detects  $p - p$  inelastic scattering in the forward direction and provides the main measurement of the relative luminosity.

The ALFA detectors (Absolute Luminosity For ATLAS) are placed  $\pm 240$  m from the IP. They consist of scintillating fibre tracking detectors located inside Roman pots which will operate at a distance of 1 mm from the beam.

The Zero-Degree Calorimeters (ZDC) are located at  $\pm 140$  m from the IP ( $|\eta| > 8.2$ ), just beyond the point where the common straight-section beam-pipe divides back into two independent beam-pipes. These calorimeters consist of layers of alternating quartz rods and tungsten plates, which will measure neutral particles; this will be particularly relevant for heavy-ion collisions.

## 2.6 Trigger and Data Acquisition

The Trigger and Data acquisition (TDAQ) system and the Detector Control System (DCS) are the fabric holding together all subdetectors and bringing the data to recording. The trigger system has three levels of filtering L1, L2 and event filter. The 40 MHz collision rate is buffered on detector pipelines (analog or digital) and held for less than  $2.5 \mu\text{s}$  while the first level trigger (compiled with coarse calorimeter and muon data) issues an L1A (L1 Accept) decision at about 75 kHz. At this point data is transmitted off the sub-detector specific ROD's (Readout Drivers) to TDAQ common infrastructure. The second L2 system works on from Regions-of-Interest (RoI's) found in L1 with full precision and granularity data and brings down the rate to  $\sim 3.5$  kHz. Finally the event filter performs an event selection delivering around 200 Hz of events with a size of  $\sim 1.3$  Mbyte to permanent storage at the CERN computer center. From there, data is distributed to Tier-1 and Tier-2 computing centers on the worldwide LHC Computing grid (wLCG).

The DCS system allows to operate the detector hardware safely and in a coherent way over all the sub-systems. It is used as interface to the shift operators which need to react on “Warnings” and “Alarms” and also the Detector Safety System (DSS) which takes automatic action when potentially dangerous events occur. It acts as interface to

the LHC accelerator and CERN technical services. Interacting with the TDAQ system, the state of the sub-detectors which might be relevant for data analysis, gets included in the data stream.

### 3 Commissioning with Cosmics and Single Beams

The commissioning of the ATLAS sub-detectors has been ongoing in parallel with the detector installation. As early as 2005, first cosmic rays were recorded with the barrel calorimeters with partially installed electronics and readout chains. Very useful information has been gradually collected for all systems using a variety of cosmic-ray triggers. This has greatly helped the commissioning of the detectors, and the initial understanding of their performance.

The main objectives of the dedicated cosmic-ray operation have been the testing of the readout of all detectors and the determination of the misbehaving channels, the studies of the operational stability of the detector hardware, further development and operation of the online software, noise studies, alignment studies, calibration operation and finally full detector operation “as with colliding beams” ... These periods of operation have been pursued in 2009, after the detector closure in the summer, and in anticipation of the LHC beams expected for late November 2009. A snapshot of the fraction of operational channels per major system at the time of these proceedings is shown in Table 2.

#### ATLAS Detector Status

Subdetector	Number of Channels	Approximate Operational Fraction
Pixels	80 M	98.0%
SCT Silicon Strips	6.3 M	99.3%
TRT Transition Radiation Tracker	350 k	98.2%
LAr EM Calorimeter	170 k	98.8%
Tile calorimeter	9800	99.5%
Hadronic endcap LAr calorimeter	5600	99.9%
Forward LAr calorimeter	3500	100%
MDT Muon Drift Tubes	350 k	99.7%
CSC Cathode Strip Chambers	31 k	98.4%
RPC Barrel Muon Trigger	370 k	>97%
TGC Endcap Muon Trigger	320 k	99.8%
LVL1 Calo trigger	7160	99.8%

Table 2: *Number of readout channels and fraction which is operational for each major ATLAS sub-detector.*

Approximately 200 million events were collected in 2008 and again in 2009, of which about ten million were triggered based on a reconstructed track in the ID (a high-level trigger). Many detector studies were performed using these data: two examples are discussed below. Finally, one last example is presented, using single beam events collected in 2008.

### 3.1 Tracking Studies with Cosmics

Cosmic muon tracks do not provide data synchronous with the 40 MHz LHC clock, nor are they usually pointing to the interaction point. They nevertheless have proven ideal to perform tracking and alignment studies with the ID and the muon spectrometer, allowing alignments of different elements within a system (modules for the ID, chambers for the muons) but also a more global alignment between the two systems. Results from such a correlation, the measurement of the polar ( $\theta$ ) and azimuthal ( $\phi$ ) angles with the ID and the muon system are shown in Figure 5 (left and center). The differences of track angles measured in each system agree well with MC predictions and show a spread of up to 10-20 mrad.

An even more interesting result is the comparison between the measurements of the muon momentum in each system. This is shown in Figure 5 (right) where the peak position and the  $\sim 3$  GeV energy loss of the muons traversing the calorimeters between the ID and the muon system are in good agreement with the MC simulations.

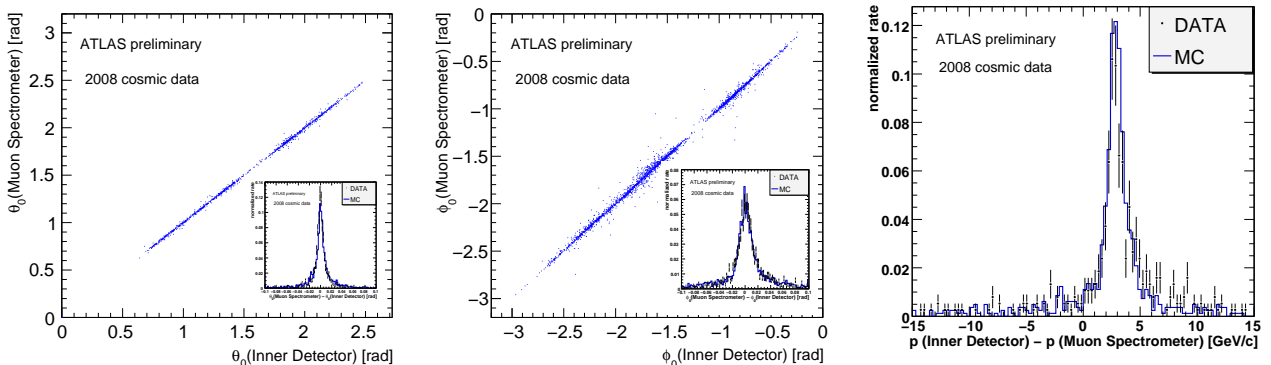


Figure 5: Correlation between muon spectrometer and ID, (left)  $\theta$  and (middle)  $\phi$ , track parameters. The differences of the angles measured in the two systems have a spread of up to 10-20 mrad, giving an idea of the cross alignment. Rightmost: difference in the muon momentum as measured in the ID and bottom part of the muon spectrometer. About 3 GeV is “lost” in the calorimeters, observed for both data and MC.

### 3.2 Calorimeter Performance with Random Events

The missing transverse energy measured in the calorimeters,  $E_T^{miss}$ <sup>1</sup> is one of the most important signatures for many physics processes. It is therefore very important to understand this quantity in the absence of particles in the detector. The  $E_T^{miss}$  measured spectrum from randomly triggered events is shown in Figure 6 where only the LAr calorimeter cells with energy above two standard deviations of the measured cell noise (in red) are added or by the more efficient noise suppression achieved by taking only cells in the standard topological clusters (in blue) [3]. The  $E_T^{miss}$  distribution is most sensitive to effects like coherent noise in the calorimeter since it potentially includes all the 180 thousand cells of the LAr calorimeter. Figure 6 demonstrates that these electronic effects are well under control. In fact, in Figure 6 (left) the tails of the distribution beyond  $\sim 8$  GeV were traced back to a particular presampler region where some cables had been wrongly shielded. This error was corrected during the 2008-09 shutdown and data from 2009 show a much reduced  $E_T^{miss}$  tail depicted in Figure 6 (right).

<sup>1</sup>  $E_T^{miss} = \sqrt{(\sum E \sin\theta \cos\phi)^2 + (\sum E \sin\theta \sin\phi)^2}$



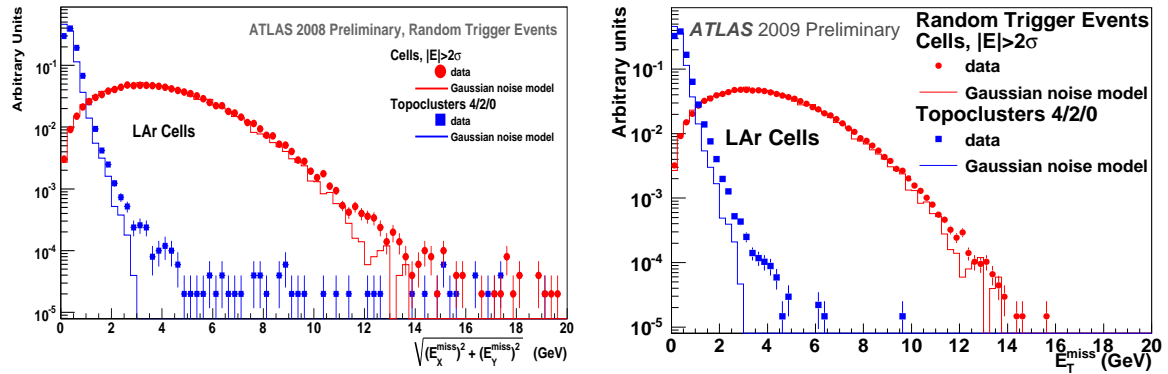


Figure 6: Measured spectra of missing transverse energy,  $E_T^{miss}$  from runs in 2008 (left) and 2009 (right).

Events taken during cosmic running data-taking and triggered by the L1 calorimeter system, clearly show excess energy deposited in the calorimeters by the muons, as illustrated in Figure 7.

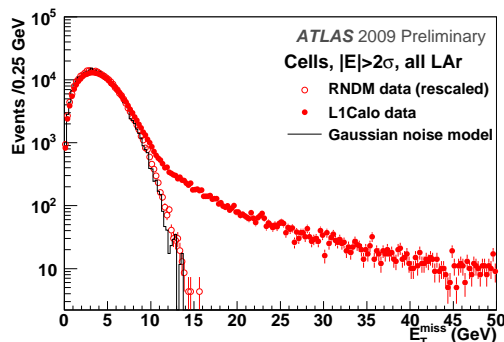


Figure 7: Measured spectra of missing transverse energy,  $E_T^{miss}$  from random triggers (RNDM) and from cosmic muons (L1Calo).

### 3.3 Calorimeter Commissioning with Single Beams

On September 10th 2008 and the following days, proton beams were circulated around the whole LHC accelerator. So-called “beam splash” events were produced by colliding the protons on closed collimators 140 m upstream of the ATLAS detector. These collisions generated a large quantity of muons reaching all parts of ATLAS and “illuminating” the whole detector at once. As an example, Figure 8 shows the energy deposits over the whole volume of the middle section of the LAr EM calorimeter. The horizontal 8-fold structure which can be guessed (but becomes apparent if projections are made) in this  $\eta - \phi$  energy plot, shows the “shadows” of the ECT coils, the most massive objects traversed by the muons produced far upstream of the experiment.

Important information for the detector start-up can be extracted from such events. For example, the timing offsets for each channel of the electronics readout, determined beforehand from cable and fiber lengths and from calibration signals can be compared to those obtained from the beam-splash particles. These comparisons are shown in Figure 9 (left) where the different points correspond to different readout sections of the EM calorimeter. After corrections for the different time-of-flights expected for beam-splash events, the predictions match the data with a precision better than 2 ns. The same is true for the Tile calorimeter (Figure 9, right) where within each section, the timing results are also uniform to better than 2 ns.

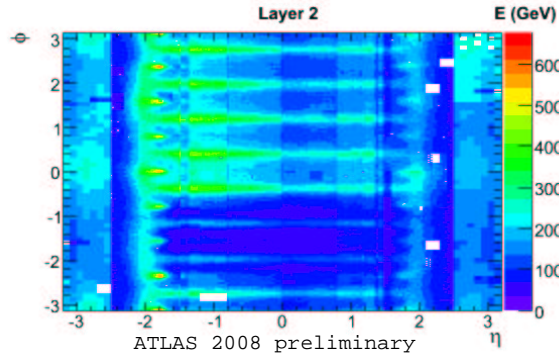


Figure 8: *Energy deposits from beam-splash events as measured in the middle layer of the LAr EM calorimeters.*

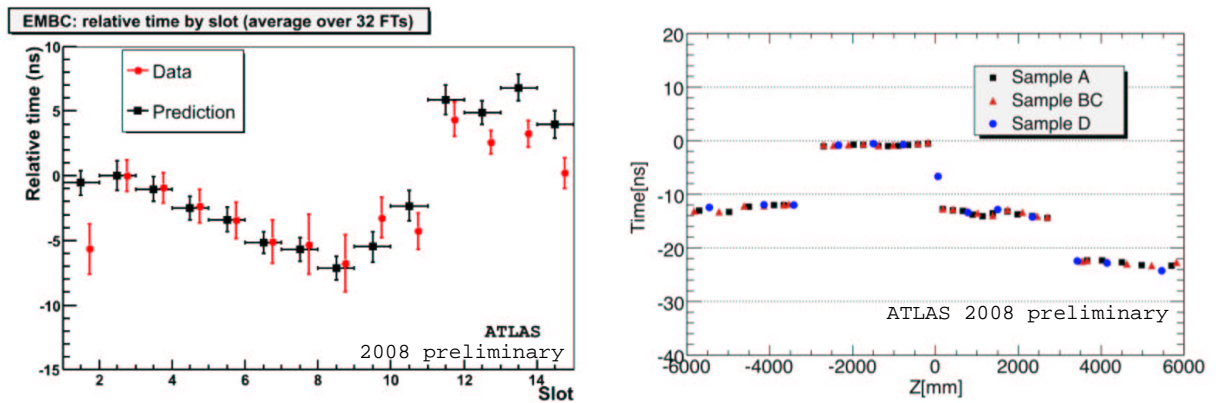


Figure 9: *Timing measurements from beam-splash events compared with predictions for LAr EM (left) and within Tile calorimeter sections (right).*

## 4 Conclusions

The ATLAS experiment at the CERN LHC has by now been globally installed, integrated and commissioned with cosmic rays and single beams. Stable operation and smooth data-taking using the readout of all systems has been achieved in 2008 and 2009 using cosmic rays. The data has been distributed to and analyzed by the whole collaboration through the world-wide computing grid. The experiment is ready for proton-proton collision data, expected in late November 2009.

## References

- [1] The ATLAS collaboration, *J. of Instr.*, 3(08):S08003 (2008).
- [2] B. Aubert et al., Development and construction of large size signal electrodes for the ATLAS electromagnetic calorimeter, *Nucl. Instrum. Meth. A* 539 (2005) 558.  
B. Aubert et al., Construction, assembly and tests of the ATLAS electromagnetic barrel calorimeter, *Nucl. Instrum. Meth. A* 558 (2006) 388.  
M. Aleksa et al., Construction, assembly and tests of the ATLAS electromagnetic end-cap calorimeter, 2008 *JINST* 3 P06002.
- [3] W. Lampl et al., Calorimeter Clustering Algorithms : Description and Performance ATLAS Note ATL-LARG-PUB-2008-002 <http://cdsweb.cern.ch/record/1099735>.